Infrared absorption in $Si/Si_{1-x}Ge_x/Si$ quantum wells

S. Ridene,[1] K. Boujdaria,[1,2] H. Bouchriha,[1] and G. Fishman[3]
[1]*Laboratoire de Physique de la Matière Condensée, Faculté des Sciences de Tunis, Université de Tunis II, Campus Universitaire, le Belvédère, 1060 Tunis, Tunisia*
[2]*Département de Physique, Faculté des Sciences de Bizerte, Université de Tunis II, 7021 Zarzouna, Bizerte, Tunisia*
[3]*Institut d'Électronique Fondamentale, UMR 8622 CNRS, Bât 220, Université Paris XI, 91405 Orsay Cedex, France*
(Received 22 February 2001; published 8 August 2001)

The infrared intersubband optical transitions in SiGe/Si quantum wells is theoretically examined. We have used the 8×8, 12×12, and 14×14 $\mathbf{k}\cdot\mathbf{p}$ Hamiltonians taking into account both the *p*-like first conduction band and the *s*-like second conduction band to calculate wave functions and energy dispersion of the valence band of $Si/Si_{0.8}Ge_{0.2}/Si$ quantum wells. We discuss intersubband absorption in the valence band and we show that the *p-p* interaction favors intersubband transitions for an optical polarization parallel to the layer plane (*x* polarization). For *z* polarization, both *s-p* and *p-p* interactions play the same footing role in intervalence band transitions.

DOI: 10.1103/PhysRevB.64.085329 PACS number(s): 73.90.+f, 78.67.De

I. INTRODUCTION

Infrared transitions in quantum well structures between either confined levels of the conduction band (CB) or confined levels of the valence band (VB), the so-called intersubband transitions, have been extensively studied during the past two decades. Most studies on this subject were based on III-V materials, especially GaAs.[1–5] It is an important matter thanks to its wide application in infrared photodetection and its use as an infrared source (quantum cascade lasers). Contrary to GaAs/AlGaAs (*n*-type) quantum wells, which needs only a polarization of the optical field along the growth direction (*z* polarization) to show the intersubband transitions,[6] GaAs/AlGaAs (*p*-type) quantum wells exhibit this intersubband transitions for both polarizations, along and across the growth direction (*x* and *z* polarization).[7] The intersubband absorption in *z*-polarization is allowed but experiments cannot be performed with a wave vector parallel to the growth direction, which makes the experiment difficult. The intersubband absorption in *x* direction is forbidden. As usual allowed and forbidden refer to transition at $\mathbf{k}_\rho=\mathbf{0}$, where $\mathbf{k}_\rho$ is the wave vector in the plane direction. The *x*-polarization absorption is possible at $\mathbf{k}_\rho\neq\mathbf{0}$ as a result of admixture between *s*-type CB and *p*-type VB (*s-p* interaction). Moreover, IV-IV heterostructures, such as $Si/Si_{1-x}Ge_x/Si$, have also been a subject of many interesting studies. One of the particularities of the quantum heterostructures $Si_{1-x}Ge_x/Si$ is associated to the band discontinuity between the two materials which occurs essentially in the VB. As a result, the observed intersubband transitions involve the different states of holes (heavy holes, light holes, and spin-orbit split VB) at $\mathbf{k}_\rho\neq\mathbf{0}$. This admixture allows to observe intersubband absorption for an optical polarization parallel to the layer plane.[8,9] The implementation of photodetector or of infrared modulator operating at normal incidence is therefore possible.[10,11] The dependence of polarization intersubband transitions in heavily doped $Si_{1-x}Ge_x/Si$ quantum well have been emphasized by Chun *et al.*[12] Many experimental investigations were recently performed in $Si_{1-x}Ge_x/Si$ quantum wells in order to study the intersubband transitions within the VB. These experiments have demonstrated the existence of the photoinduced intersubband absorption in doped or undoped wells.[13,14]

These intersubband transitions show strong dipolar moment, which is convenient for observation of important nonlinear effects. Nonlinear second-order optical resonant transitions of harmonic generation at 10.6 μm in asymmetrical wells have been observed.[15] The saturation of intersubband absorption in the VB at 10 μm and the measurement of intersubband relaxation time have been emphasized in Ref. 16. Additionally, Ref. 17 points out studies on the evolution of the intersubband absorption in interdiffused $Si_{1-x}Ge_x/Si$ quantum wells. The most realistic approach to analyze and model the experimental results is to consider a full description of the quantum well band structure. Furthermore, a large variety of methods for studying the pertinent experiments have been reported in the literature, such as the pseudopotential method[18] and the computation of the dispersion in the valence band taking into account the coupling between the three VB, heavy holes, light holes, and spin orbit.[19] As quoted in Ref. 20, "detailed calculations of the transitions strengths away from the zone center would be necessary." The purpose of this paper is to show another theoretical aspect on the oscillator strengths.

Up to now the admixture between the $\Gamma_5^+/(\Gamma_8^+ + \Gamma_7^+)$ in simple/double group VB and the Γ_2^-/Γ_7^- CB was calculated taking into account the *s*-like (Γ_2^-) CB. This is justified for semiconductors such as GaAs or Ge where the Γ_2^- CB is the lowest CB. This leads to use a 8×8 H_8 Hamiltonian (6 for the Γ_5^+ VB, 2 for the Γ_2^- CB). However, in silicon or in $Si_{1-x}Ge_x$ with a small Ge concentration the lowest CB has the $\Gamma_4^-/(\Gamma_8^- + \Gamma_6^-)$ symmetry and the use of the H_8 is no longer justified. The use of H_8 would be justified if the optical matrix element between the $\Gamma_5^+/(\Gamma_8^+ + \Gamma_7^+)$ and Γ_4^- would be zero or very small with respect to the matrix element between Γ_5^+ and Γ_2^-. However, the square of the first matrix element is larger than half the square of the second one,[21] i.e., both matrix elements are of the same order of magnitude. Thus, in $Si_{1-x}Ge_x$, we have to take into account

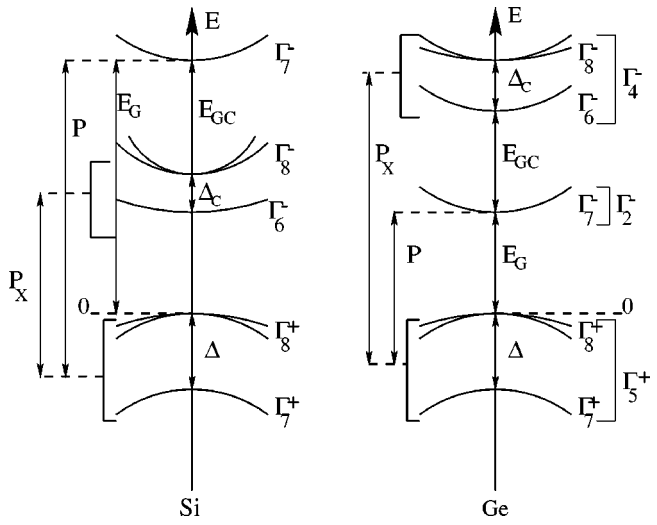

FIG. 1. Five-level model (14-level model by taking into account the spin-orbit coupling) for Si and Ge near the Γ point of the Brillouin zone. The notation of (i) the energy gaps E_G, E_{GC}, (ii) the spin orbit splittings Δ and Δ_C, and (iii) the interband matrix elements of momentum P and P_X useful here are symbolically indicated. The numerical values of E_G, E_{GC}, Δ, and Δ_C are given in Table I.

both bands Γ_4^- and Γ_2^- on the same foot. Indeed, one of the aims of this paper is to show the influence of the first two CB's, namely Γ_2^- and Γ_4^-, on intersubband absorption with normal incidence for a 34 Å $Si_{0.8}Ge_{0.2}/Si$ strained quantum well. First we begin to study the oscillator strengths taking into account Γ_5^+ and Γ_2^- levels via the H_8 Hamiltonian. Second we take into account Γ_5^+ and Γ_4^- levels via a 12×12 H_{12} Hamiltonian (6 for the Γ_4^- CB). Finally we take into account all the levels Γ_5^+, Γ_4^- and Γ_2^- via a 14×14 Hamiltonian H_{14}. From a numerical viewpoint we use a method which has been shown efficient in studies of several kinds of two and one dimensional semiconductors.[22–24]

The method used here for calculating electronic band structure is based on the 14×14 $\mathbf{k}\cdot\mathbf{p}$ method.[25] This method has been used previously for calculating the electronic band structure in the bulk semiconductors.[26–29] The most complete treatment along these lines has been detailed by Pfeffer and Zawadzki[21,30] who described in detail various properties of conduction electrons in GaAs and determined important band parameters. The layout of this paper is as follows: In Sec. II we give the theoretical $\mathbf{k}\cdot\mathbf{p}$ framework account for the Γ_5^+, Γ_4^-, and Γ_2^- levels. In Sec. III we give the dispersion relations obtained with the three above Hamiltonians. The dependence of intersubband absorption versus the wave vector and the absorption ratio calculated between x and z polarizations versus the wave vector is given in Sec. IV. The Sec. V is devoted to the conclusion.

II. QUANTUM WELL STRUCTURE

A. The Hamiltonian matrix elements

In the absence of strain, the band structure can be found by solving the $\mathbf{k}\cdot\mathbf{p}$ equation:[31]

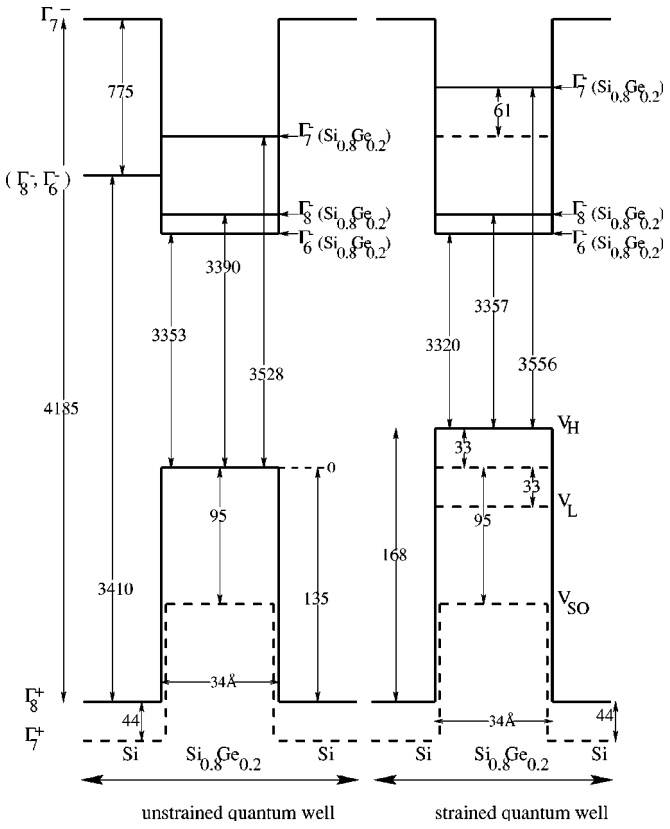

FIG. 2. The band structure of the unstrained $Si_{0.8}Ge_{0.2}/Si$ quantum well and of the strained $Si_{0.8}Ge_{0.2}$ quantum well grown on Si (001) with a well width of 34 Å. The energies are given in meV and the zero energy is taken at the top of the unstrained heavy-hole well.

$$H_k U_{lk}^{(0)} = E_{\not k}^{(0)}(k) U_{lk}^{(0)}, \tag{1}$$

where

$$H_k = \frac{\mathbf{p}^2}{2m_0} + \mathfrak{U} + \frac{\hbar}{4m_0^2c^2}(\vec{\nabla}\mathfrak{U}\wedge\vec{p})\cdot\vec{\sigma} + \frac{\hbar}{m_0}k\cdot p + \check{k}^2 \tag{2}$$

and m_0 is the free electron mass, $\mathfrak{U}$ is the periodic potential of the unstrained crystal, $\check{k}^2=\hbar^2k^2/2m_0$ and $\vec{\sigma}=(\sigma_x,\sigma_y,\sigma_z)$ are the Pauli matrices. $U_{lk}^{(0)}$ denotes Bloch spinors in the unstrained crystal. Standard notation is used for the other quantities. In Eq. (2) we have neglected $\hbar/4m_0^2c^2(\vec{\nabla}\mathfrak{U}\wedge\vec{k})\cdot\vec{\sigma}$ term which gives rise to k linear terms in semiconductors without inversion center such as GaAs. In the following, we applied the $\mathbf{k}\cdot\mathbf{p}$ formalism to the 14 fold space of the VB $(\Gamma_8^+ + \Gamma_7^+)$, the lowest (Γ_7^-) and the second CB $(\Gamma_8^- + \Gamma_6^-)$ which are treated as quasidegenerate. In Appendix A H_k is given explicity for $k=(k_x,k_y,k_z)$. However, in our calculations, inside the $\Gamma_8^- + \Gamma_6^-$ CB, we have taken all the off-diagonal interaction terms including the p-type CB's equal to zero. Figure 1 gives the band structure of interest in silicon and germanium.

TABLE I. Numerical values of bulk parameters used in this work for Si and Ge. The energies gap E_G and E_{GC}, spin orbit splitting Δ and Δ_C, Kane energy E_P, and the energy E_{PX} are given in eV. The γ_j's ($j=1,2,3$) are the Luttinger parameters and m_c is the effective masses (in m_0) at band edge of type Γ_2^-. All parameters are obtained from Ref. 34, except for the energy E_{PX} which is obtained by $E_{PX}=3(\gamma_3-\gamma_2)(E_G+E_{GC})$. This later relation is obtained via the twenty $\mathbf{k}\cdot\mathbf{p}$ model (Ref. 39).

	E_G	E_{GC}	Δ	Δ_C	E_P	E_{PX}	γ_1	γ_2	γ_3	m_C
Si	4.185	−0.775	0.044	0	21.60	11.32	4.285	0.339	1.446	0.528
Ge	0.898	2.225	0.297	0.186	26.30	13.58	13.38	4.24	5.69	0.038

B. The k·p method of a strained-layer quantum wells

The band structure in the presence of strain (for any k in the Brillouin zone) can be found using the method reported by Pikus and Bir.[32] The strain matrix element H_S can be obtained from the $\mathbf{k}\cdot\mathbf{p}$ matrix element (see Appendix A). It can be easily included by the same symmetry consideration and a straightforward addition of corresponding terms: $k_\alpha k_\beta \rightarrow \varepsilon_{\alpha\beta}$; $\alpha,\beta=x,y,z$ ($\varepsilon_{\alpha\beta}$ have exactly the same symmetry as $k_\alpha k_\beta$) with the deformation potentials a_c, a_v, and b_v, at the corresponding positions of $\tilde{\gamma}_c/2$, $-\tilde{\gamma}_1/2$ (or $-\tilde{\gamma}_{\Delta 1}/2$) and $-\tilde{\gamma}_2$ (or $-\tilde{\gamma}_{\Delta 2}$). The problem under consideration is that of a quantum well grown on (001) substrate, in which the well material is thin enough so that it can elastically accommodate the strain due to lattice mismatch. Under these conditions, the strain in the (001) plane is

$$\varepsilon_{xx}=\varepsilon_{yy}=\varepsilon_{\parallel}=\frac{a_{(Si)}-a_{(Si_{1-x}Ge_x)}}{a_{(Si_{1-x}Ge_x)}}, \tag{3}$$

where $a_{(Si)}$ and $a_{(Si_{1-x}Ge_x)}$ are the lattice constants of the substrate (barrier material) and the layer material (well material), respectively. The condition of zero stress in the z direction yields

$$\varepsilon_{zz}=\varepsilon_{\perp}=-2\frac{C_{12}}{C_{11}}\varepsilon_{\parallel}, \tag{4}$$

while $\varepsilon_{xy}=\varepsilon_{yz}=\varepsilon_{zx}=0$. C_{11} and C_{12} are the elastic stiffness constants. The 8×8 strain Hamiltonian matrix, namely H_S matrix which is well known,[33] induces a shift and a splitting from the potential V due to both VB and CB offset, so that the well for light holes is not the same as for heavy holes. The subband dispersion was obtained from a second order $\mathbf{k}\cdot\mathbf{p}$ 14-band Hamiltonian (A1) H_k onto which we expanded the 8×8 strain Hamiltonian H_S and the potential V. The Hamiltonian to be solved is

TABLE II. This table gives the values of the lattice parameter a (in Å) for Si and Ge. The deformation potentials a_c for the CB and a_v, b_v for the VB are given in eV. $a_g=a_c-a_v$ is the gap deformation potential. C_{11} and C_{12} are the elastic moduli (stiffnesses) given in MPa. All parameters are obtained from Ref. 34.

	a	a_c	a_v	a_g	b_v	C_{11}	C_{12}
Si	5.431	−5.10	0	−5.10	−2.10	1.675	0.65
Ge	5.658	−9.50	0	−9.50	−2.90	1.315	0.494

$$H=H_k+H_S+V(z), \tag{5}$$

where $V(z)$, which is a scalar, is diagonal in the 14-dimensional spinor basis. In unstrained semiconductors $V(z)$ describes only the valence and conduction band offset. In strained semiconductors the whole potential results from both the chemical potential $V(z)$ and the potential induced by the strain H_S. Figure 2 gives the band structure of unstrained and strained $Si/Si_{0.8}G_{0.2}/Si$ quantum well.

III. k·p THEORY: VALENCE DISPERSION CURVES

Calculations for valence-subband structure can be carried out with the methods outlined in the previous section. In our calculation we have taken linear interpolation of all parameters. The Si and SiGe band parameters have been taken from Ref. 34 (Tables I and II) and a heavy-hole valence band offset $\Delta E_V=840x$ (meV) (Ref. 35) has been assumed. We choose the quantum well direction (z axis) as the quantization axis of the angular momentum. Figure 3 shows the valence-subband structure of 34 Å $Si_{0.8}Ge_{0.2}/Si$ strained quantum well obtained with the axial approximation.[36] The optical properties of these quantum well will be discussed extensively below. At the zone center ($\mathbf{k}_\rho=\mathbf{0}$), the valence subbands are either heavy-hole (H_n)-like, light-hole

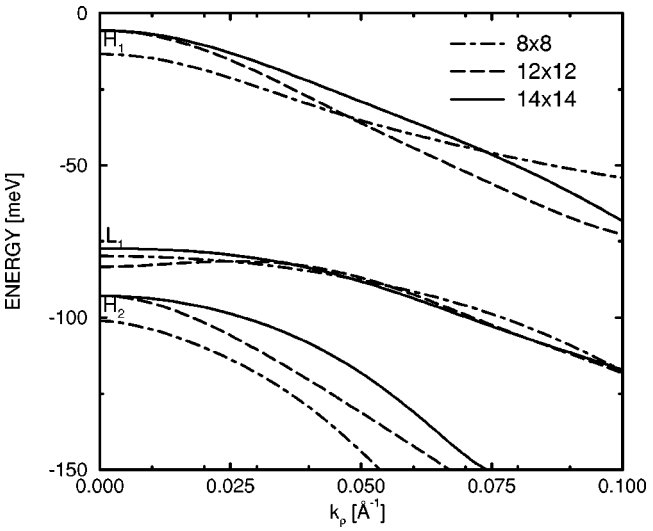

FIG. 3. Valence-subband structure of a 34 Å quantum well of $Si_{0.8}Ge_{0.2}/Si$, along the [001] direction, calculated with 14×14 Hamiltonian model (solid lines), 12×12 Hamiltonian model (long-dashed lines), and 8×8 Hamiltonian model (dot-dashed lines).

TABLE III. Luttinger-Kohn periodic amplitudes used in 14-bands model. For convenience, the functions phases are chosen arbitrarily for several reasons (hole functions, maximum of matrix elements are real).

$\|c\frac{3}{2}\rangle=\|i\left[-\frac{1}{\sqrt{2}}(X_c+iY_c)\uparrow\right]\rangle$	$\|\frac{3}{2}\rangle=\|i\left[-\frac{1}{\sqrt{2}}(X+iY)\uparrow\right]\rangle$
$\|c\frac{1}{2}\rangle=\|i\left[\sqrt{\frac{2}{3}}Z_c\uparrow-\frac{1}{\sqrt{6}}(X_c+iY_c)\downarrow\right]\rangle$	$\|\frac{1}{2}\rangle=\|i\left[\sqrt{\frac{2}{3}}Z\uparrow-\frac{1}{\sqrt{6}}(X+iY)\downarrow\right]\rangle$
$\|c-\frac{1}{2}\rangle=\|i\left[\frac{1}{\sqrt{6}}(X_c-iY_c)\uparrow+\sqrt{\frac{2}{3}}Z_c\downarrow\right]\rangle$	$\|-\frac{1}{2}\rangle=\|i\left[\frac{1}{\sqrt{6}}(X-iY)\uparrow+\sqrt{\frac{2}{3}}Z\downarrow\right]\rangle$
$\|c-\frac{3}{2}\rangle=\|i\left[\frac{1}{\sqrt{2}}(X_c-iY_c)\downarrow\right]\rangle$	$\|-\frac{3}{2}\rangle=\|i\left[\frac{1}{\sqrt{2}}(X-iY)\downarrow\right]\rangle$
$\|c\frac{7}{2}\rangle=\|i\left[\frac{1}{\sqrt{3}}Z_c\uparrow+\frac{1}{\sqrt{3}}(X_c+iY_c)\downarrow\right]\rangle$	$\|\frac{7}{2}\rangle=\|i\left[\frac{1}{\sqrt{3}}Z\uparrow+\frac{1}{\sqrt{3}}(X+iY)\downarrow\right]\rangle$
$\|c-\frac{7}{2}\rangle=\|i\left[\frac{1}{\sqrt{3}}(X_c-iY_c)\uparrow-\frac{1}{\sqrt{3}}Z_c\downarrow\right]\rangle$	$\|-\frac{7}{2}\rangle=\|i\left[\frac{1}{\sqrt{3}}(X-iY)\uparrow-\frac{1}{\sqrt{3}}Z\downarrow\right]\rangle$
$\|+\rangle=\|S\uparrow\rangle$	$\|-\rangle=\|S\downarrow\rangle$

(L_n)-like or spin-orbit-like, and they are labeled H_1, "L_1," H_2, "L_2," "SO_1," etc., according to their characters and principal quantum numbers. "L_n" and "SO_n" indicate that, even at $\mathbf{k}_\rho=\mathbf{0}$, the functions are not pure $|\pm\frac{1}{2}\rangle$ and $|\pm\frac{7}{2}\rangle$ but they are mixed ($|\pm\frac{1}{2}\rangle$ and $|\pm\frac{7}{2}\rangle$ are defined in Table III). As shown in Fig. 3 and for the three Hamiltonian model (8×8, 12×12, or 14×14) there is very little band admixture in the dispersions since we are dealing with a material having wide band gap. At large values of $\mathbf{k}_\rho$, the highest light-hole band "L_1" and the two highest heavy-hole bands H_1 and H_2 are mixed leading to strongly nonparabolic dispersions relations. For example, a strong coupling between the two states "L_1" and H_1 for 12×12 Hamiltonian model is observed near $\mathbf{k}_\rho=\mathbf{0}$. This indicates the valence bands are strongly mixed between them as well as with the conduction band in the quantum well. For the two Hamiltonian model (12×12 or 14×14), we note that the energy of the heavy-hole branches at $\mathbf{k}_\rho=\mathbf{0}$ are the same (they are coupled in the same way with the other branches), but the light-hole branches are pulled up. The curvatures of all branches are strongly dependent on the Hamiltonian model (8×8, 12×12, or 14×14) and as a consequence, they will present different effective masses.

IV. INTERSUBBAND TRANSITION

After the states and energies of the semiconductor heterostructure system have been calculated via the $\mathbf{k}\cdot\mathbf{p}$ method described in the previous sections, optical transitions between the valence band states (intervalence band transitions) can then be evaluated. For evaluating the momentum matrix element between initial state $|\Psi_{H_1,k_\rho,3/2}\rangle$ and final state $|\Psi_{H_2,k_\rho,3/2}\rangle$, one needs to calculate the term:

$$(\vec{u}\cdot\vec{p})_{H_1\to H_2}=\langle\Psi_{H_1,k_\rho,3/2}|\vec{u}\cdot\vec{p}|\Psi_{H_2,k_\rho,3/2}\rangle, \tag{6}$$

where $\vec{u}$ is a unit vector in the direction of the electric field. The valence-subband states $|\Psi_{H_i,k_\rho,3/2}\rangle$ $(i=1,2)$ with wave vector k_ρ can be expanded in terms of a set of basis states $|M\rangle$ ($|M\rangle$ are the 14 basis functions represented by the $|J,M_J\rangle$ notation):

$$|\Psi_{H_i,k_\rho,3/2}\rangle=\sum_M e^{i\boldsymbol{\rho}\cdot\mathbf{k}_\rho}\chi_M^{H_i}(z)|M\rangle, \tag{7}$$

where $\rho=(x,y)$. Finally, for $\chi_M^{H_i}(z)$ we take the following expansion:

$$\chi_M^{H_i}(z)=\frac{1}{\sqrt{A}}\sum_l C_l^M\sin\left(\frac{l\pi z}{2A}\right), \tag{8}$$

where $2A$ is the quantum well width and we take $|\phi_l\rangle=(1/\sqrt{\mathbf{A}})\sin(l\pi z/2A)$ as the basis.[22] Using the expansion as given in Eqs. (7) and (8) into Eq. (6), we have

$$(\vec{u}\cdot\vec{p})_{H_1\to H_2}=\sum_{M_1M_2}\left\{\begin{array}{c}\hbar\vec{k}_\rho\cdot\vec{u}\,\delta_{M_1,M_2}\langle\chi_{M_1}^{H_1}|\chi_{M_2}^{H_2}\rangle+\langle\chi_{M_1}^{H_1}|u_zp_z|\chi_{M_2}^{H_2}\rangle\delta_{M_1,M_2}\\+\langle\chi_{M_1}^{H_1}|\chi_{M_2}^{H_2}\rangle\langle M_1|\vec{u}\cdot\vec{p}|M_2\rangle\end{array}\right\} \tag{9}$$

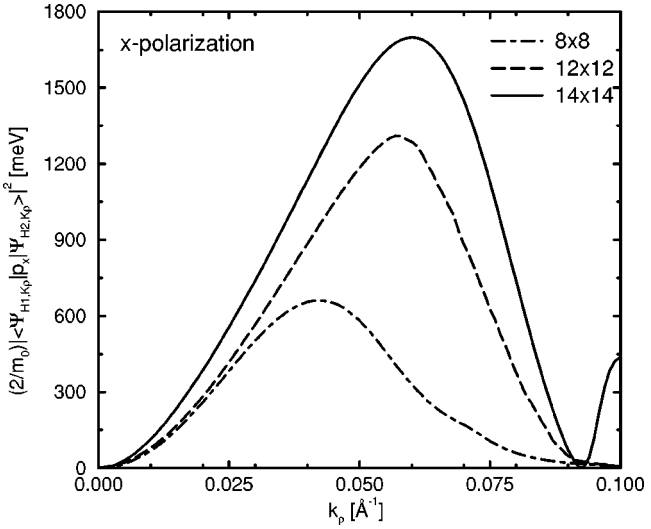

FIG. 4. Squared momentum matrix elements for a light polarized along the x direction between sublevels H_1 and H_2 in a 34 Å $Si_{0.8}Ge_{0.2}/Si$ strained quantum well. Dot-dashed line, long-dashed line, and solid line give the result respectively with H_8 Hamiltonian taking into account the bands $\{\Gamma_5^+,\Gamma_2^-\}$, with the H_{12} Hamiltonian taking into account the bands $\{\Gamma_5^+,\Gamma_4^-\}$ and with the H_{14} Hamiltonian taking into account the bands $\{\Gamma_5^+,\Gamma_4^-,\Gamma_2^-\}$ (see text).

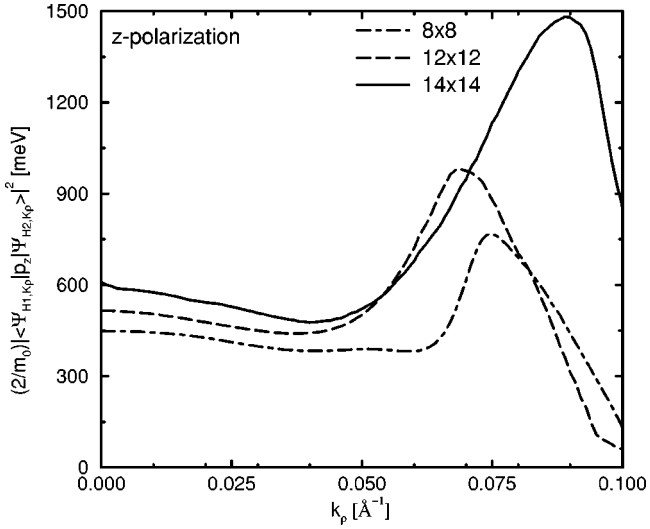

FIG. 5. Same as in Fig. 4 but for a light polarized along the z direction.

the optical matrix $\vec{u}\cdot\vec{p}$ in Eq. (9) can be obtained from the $\mathbf{k}\cdot\mathbf{p}$ matrix element given in Sec. II. The optical matrix has indeed the same form as the $\mathbf{k}\cdot\mathbf{p}$ matrix element, except that k_ik_j is replaced with $k_iu_j+k_ju_i$. The coefficients of the overlap terms in Eq. (9) are linear in $\mathbf{k}_\rho$, whereas the coefficients of the dipole terms are independent of $\mathbf{k}_\rho$. Further the overlap terms only couples envelope functions of the same parity, whereas the dipole terms only couples envelope functions of opposite parities. The form of Eq. (9) shows that the x-polarization absorption is going to be different to zero if the initial or the final state has a p symmetry. If the Hamiltonian described only the p symmetry VB or the p symmetry CB, the optical matrix element would simply be a zero, so that at $\mathbf{k}_\rho=\mathbf{0}$ the two highest heavy-hole states $|\Psi_{H_i,k_\rho,3/2}\rangle$ $(i=1,2)$ are completely decoupled with all the conduction subband states. Figures 4 and 5 show the squared momentum matrix elements $(2/m_0)|\langle\Psi_{H_1,k_\rho,3/2}|\vec{u}\cdot\vec{p}|\Psi_{H_2,k_\rho,3/2}\rangle|^2$ for a 34 Å $Si_{0.8}Ge_{0.2}/Si$ strained quantum well versus the plane wave vector for x- and z-polarized fields, respectively. In both of these figures a prominent transition from the first subband H_1 to the three subband H_2 is shown. For convenience, $(H_1H_2)_{8\times8}$ is defined as the transition when the initial state is H_1, the final state is H_2 and to calculate with eightfold space of Γ_7^-, Γ_8^+, and Γ_7^+. We note that in our notation, (12×12) means that the $\mathbf{k}\cdot\mathbf{p}$ formalism is applied inside the p-CBs and the p-VBs. For the x polarization, as shown in Fig. 5, $(H_1H_2)_{14\times14}$ are very strong for $\mathbf{k}_\rho$ peaks around 0.06 Å^{-1} and decreases when $\mathbf{k}_\rho$ increases. $(H_1H_2)_{12\times12}$ offers the same behavior and exhibits a peak around 0.06 Å^{-1} as well. Thus we expect the (H_1-H_2) transition at $\mathbf{k}_\rho=0.06$ Å^{-1} to play an important role in the absorption. $(H_1H_2)_{8\times8}$ transition shows a broadness peak around $\mathbf{k}_\rho=0.04$ Å^{-1}. The broadness of the intersubband transition peaks is partially due to the nonparabolic behavior of the valence subbands. The $(H_1H_2)_{12\times12}$ transition is twice stronger than $(H_1H_2)_{8\times8}$ one. This fact indicates that the coupling between the p-type CB's and p-type VB's (p-p coupling) plays an important role for the x-polarization intersubband transition. For the z polarization, as shown in Fig. 5, $(H_1H_2)_{8\times8}$ and $(H_1H_2)_{12\times12}$ are strong at the zone center and becomes large for $\mathbf{k}_\rho\approx0.07$ Å^{-1}. For $\mathbf{k}_\rho<0.08$ Å^{-1}, the $(H_1H_2)_{8\times8}$ transition is similar to $(H_1H_2)_{12\times12}$ one and the peak position is around $\mathbf{k}_\rho\approx0.075$ Å^{-1}. However, the peak position for $(H_1H_2)_{12\times12}$ transition moves slightly to a lower $\mathbf{k}_\rho$ (0.069 Å^{-1}). The peak intensity of the squared

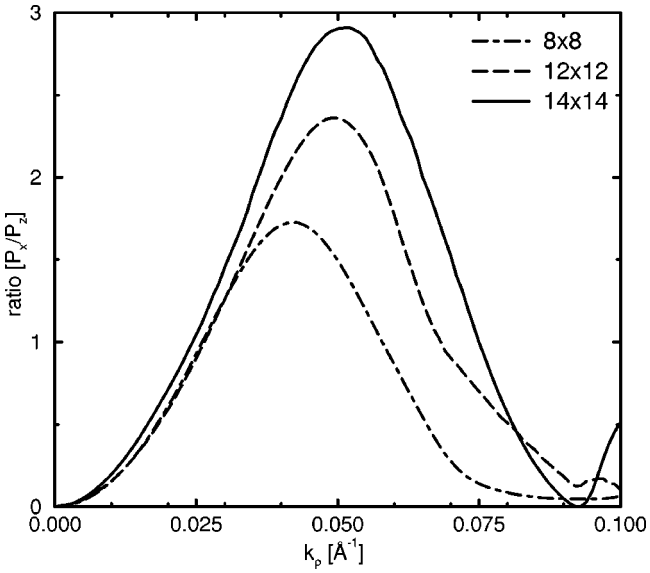

FIG. 6. The ratio between squared momentum matrix elements for x and z polarization for the H_1-H_2 transitions versus the plane wave vector k_ρ. Dot-dashed line, long-dashed line and solid line give the result respectively with H_8 Hamiltonian, H_{12} Hamiltonian, and H_{14} Hamiltonian.

momentum matrix for (8×8) case is about 765 meV, whereas the (12×12) one is about 980 meV. The squared momentum matrix in both these two Hamiltonian models are almost identical, and therefore, so are the calculated intensities for each optical transition. This indicates that the $(s\text{-}p)$ coupling and the $(p\text{-}p)$ coupling play an equal footing role for the z polarization. In the (14×14) case, a peak position is found at near 0.09 Å^{-1} and the peak intensity is about 1500 meV, approximately the sum of the two transition cases $(8\times8$ and $12\times12)$. Figure 6 shows the ratio between squared momentum matrix elements for x and z polarization for the $(H_1\text{-}H_2)$ transitions versus the plane wave vector $\mathbf{k}_\rho$. As expected from momentum matrix element in Fig. 4 and Fig. 5, the ratio $[P_x/P_z]_{14\times14}$ is stronger than the $[P_x/P_z]_{12\times12}$ one which is stronger than the $[P_x/P_z]_{8\times8}$ one. For (8×8) Hamiltonian model, absorption of x-polarized light could be stronger than that of z-polarized beam if $\mathbf{k}_\rho$ belongs to $[0.025\ \text{Å}^{-1},\ 0.06\ \text{Å}^{-1}]$. This indicates that inside this $\mathbf{k}_\rho$ interval, the forbidden transition becomes much stronger than the allowed transition. For (12×12) Hamiltonian model, the $\mathbf{k}_\rho$ interval where $[P_x/P_z]_{12\times12}>1$ is more wide for the one calculated with (8×8) Hamiltonian model. Moreover, the intensity ratio for the (12×12) Hamiltonian model is more stronger that the (8×8) one. This is explained by the fact that the anisotropic interaction $p\text{-}p$ favors the intersubband transitions for a radiation electric field parallel to the layers rather than for an electric field along the growth direction.

V. CONCLUSION

The intersubband transitions in the VB were calculated for x and z polarization. We have presented a general five-levels $\mathbf{k}\cdot\mathbf{p}$ model in which one takes explicitly into account the p-symmetry VB and the s- and p-symmetry CB's. We have calculated the dispersion relation of valence subband in the axial approximation for a strained semiconductors quantum well. We have given the intersubband absorption of strained $Si_{0.8}Ge_{0.2}/Si$ quantum well for the x and z polarization. Our calculation clearly explains that the anisotropic $p\text{-}p$ interaction favors the x polarization, whereas the isotropic interaction $(s\text{-}p$ interaction) and the anisotropic one play an equal footing role for the z polarization.

ACKNOWLEDGMENTS

We would like to thank Philippe Boucaud for useful discussions. This work was supported in part by the contract DGRST/CNRS Code 98/R1304. We wish to thank the El Khawarizmi Computing Center at El Manar, Tunis, where our numerical computations were done.

APPENDIX A: H_k MATRIX

In the basis spinors at $\mathbf{k}=\mathbf{0}$ given in Appendix B (see Table III) (taken in order: $|c\tfrac{3}{2}\rangle$, $|c\tfrac{1}{2}\rangle$, $|c-\tfrac{1}{2}\rangle$, $|c-\tfrac{3}{2}\rangle$, $|c\tfrac{7}{2}\rangle$, $|c-\tfrac{7}{2}\rangle$, $|+\rangle$, $|-\rangle$, $|\tfrac{3}{2}\rangle$, $|\tfrac{1}{2}\rangle$, $|-\tfrac{1}{2}\rangle$, $|-\tfrac{3}{2}\rangle$, $|\tfrac{7}{2}\rangle$, $|-\tfrac{7}{2}\rangle$), the 14×14 $\mathbf{k}\cdot\mathbf{p}$ Hamiltonian H_k is given by

$$\mathbf{H}_k=\begin{pmatrix}
E_{8C}^{+0} & \mathfrak{B}_C & \mathfrak{C}_C & 0 & \frac{1}{\sqrt{2}}\mathfrak{B}_{\Delta C} & \sqrt{2}\mathfrak{C}_{\Delta C} & 0 & 0 & 0 & \frac{1}{\sqrt{3}}P_X^+ & \frac{1}{\sqrt{3}}P_X^z & 0 & \frac{1}{\sqrt{6}}P_X^+ & \sqrt{\frac{2}{3}}P_X^z \\
cc & E_{8C}^{-0} & 0 & \mathfrak{C}_C & -\sqrt{2}\mathfrak{A}_{\Delta C} & -\sqrt{\frac{3}{2}}\mathfrak{B}_{\Delta C} & 0 & 0 & \frac{-1}{\sqrt{3}}P_X^- & 0 & 0 & \frac{1}{\sqrt{3}}P_X^z & 0 & \frac{-1}{\sqrt{2}}P_X^+ \\
cc & 0 & E_{8C}^{-0} & -\mathfrak{B}_C & -\sqrt{\frac{3}{2}}\mathfrak{B}_{\Delta C}^* & \sqrt{2}\mathfrak{A}_{\Delta C} & 0 & 0 & \frac{-1}{\sqrt{3}}P_X^z & 0 & 0 & \frac{-1}{\sqrt{3}}P_X^+ & \frac{1}{\sqrt{2}}P_X^- & 0 \\
0 & cc & cc & E_{8C}^{+0} & -\sqrt{2}\mathfrak{C}_{\Delta C}^* & \frac{1}{\sqrt{2}}\mathfrak{B}_{\Delta C}^* & 0 & 0 & 0 & \frac{-1}{\sqrt{3}}P_X^z & \frac{1}{\sqrt{3}}P_X^- & 0 & \sqrt{\frac{2}{3}}P_X^z & \frac{-1}{\sqrt{6}}P_X^- \\
cc & cc & cc & cc & E_{7C}^0 & 0 & 0 & 0 & \frac{-1}{\sqrt{6}}P_X^- & 0 & \frac{-1}{\sqrt{2}}P_X^+ & -\sqrt{\frac{2}{3}}P_X^z & 0 & 0 \\
cc & cc & cc & cc & 0 & E_{7C}^0 & 0 & 0 & -\sqrt{\frac{2}{3}}P_X^z & \frac{1}{\sqrt{2}}P_X^- & 0 & \frac{1}{\sqrt{6}}P_X^+ & 0 & 0 \\
0 & 0 & 0 & 0 & 0 & 0 & E_6^0 & 0 & \frac{-1}{\sqrt{2}}P^+ & \sqrt{\frac{2}{3}}P^z & \frac{1}{\sqrt{6}}P^- & 0 & \frac{1}{\sqrt{3}}P^z & \frac{1}{\sqrt{3}}P^- \\
0 & 0 & 0 & 0 & 0 & 0 & 0 & E_6^0 & 0 & \frac{-1}{\sqrt{6}}P^+ & \sqrt{\frac{2}{3}}P^z & \frac{1}{\sqrt{2}}P^- & \frac{1}{\sqrt{3}}P^+ & \frac{-1}{\sqrt{3}}P^z \\
0 & cc & cc & 0 & cc & cc & cc & 0 & E_8^{+0} & \mathfrak{B} & \mathfrak{C} & 0 & \frac{1}{\sqrt{2}}\mathfrak{B}_\Delta & \sqrt{2}\mathfrak{C}_\Delta \\
cc & 0 & 0 & cc & 0 & cc & cc & cc & cc & E_8^{-0} & 0 & \mathfrak{C} & -\sqrt{2}\mathfrak{A}_\Delta & -\sqrt{\frac{3}{2}}\mathfrak{B}_\Delta \\
cc & 0 & 0 & cc & cc & 0 & cc & cc & cc & 0 & E_8^{-0} & -\mathfrak{B} & -\sqrt{\frac{3}{2}}\mathfrak{B}_\Delta^* & \sqrt{2}\mathfrak{A}_\Delta \\
0 & cc & cc & 0 & cc & cc & 0 & cc & 0 & cc & cc & E_8^{+0} & -\sqrt{2}\mathfrak{C}_\Delta^* & \frac{1}{\sqrt{2}}\mathfrak{B}_\Delta^* \\
cc & 0 & cc & cc & 0 & 0 & cc & cc & cc & cc & cc & cc & E_7^0 & 0 \\
cc & cc & 0 & cc & 0 & 0 & cc & cc & cc & cc & cc & cc & 0 & E_7^0
\end{pmatrix}, \tag{A1}$$

where

$$\check{k}_j^2=\frac{\hbar^2 k_j^2}{2m_0}, j=x,y,z;\ \ k_{\pm}=k_x\pm ik_y;\ \ P^z=Pk_z;\ \ P^{\pm}=Pk_{\pm};\ \ P_X^z=P_Xk_z;\ \ P_X^{\pm}=P_Xk_{\pm}.$$

Taking the zero of energy at the top of the Γ_8^+, one obtains

$$E_{8C}^{+0}=E'_{8C}-\tilde{\gamma}_{C1}\check{k}^2+\mathfrak{A}_C,$$

$$E_{8C}^{-0}=E'_{8C}\cdots\tilde{\gamma}_{C1}\check{k}^2\cdots\mathfrak{A}_C,$$

$$E_{7C}^{0}=E'_{7C}-\tilde{\gamma}_{\Delta C1}\check{k}^2,$$

$$E_6^0=E_6+\tilde{\gamma}_C\check{k}^2,$$

$$E_8^{+0}=E'_8-\tilde{\gamma}_1\check{k}^2+\mathfrak{A},$$

$$E_8^{-0}=E'_8-\tilde{\gamma}_1\check{k}^2-\mathfrak{A},$$

$$E_7^0=E'_7-\tilde{\gamma}_{\Delta 1}\check{k}^2,$$

where

$$E'_{8C}=E_G+E_{GC}+\Delta_C,$$

$$E'_{7C}=E_G+E_{GC},$$

$$E_6=E_G,$$

$$E'_8=0,$$

$$E'_7=-\Delta.$$

The spin-orbit energies are defined as

$$\Delta=\frac{3\hbar}{4m_0^2c^2}\langle iX|[\vec{\nabla}\mathfrak{U}\wedge\vec{p}]_y|Z\rangle;\Delta_C=\frac{3\hbar}{4m_0^2c^2}\langle iX_C|[\vec{\nabla}\mathfrak{U}\wedge\vec{p}]_y|Z_C\rangle$$

and the momentum matrix elements are

$$P=\langle S|p_x|iX\rangle,$$

$$P_X=\langle X_C|p_z|iY\rangle=\langle Y_C|p_z|iX\rangle=\langle X_C|p_y|iZ\rangle=-\langle X|p_z|iY_C\rangle=-\langle Y|p_z|iX_C\rangle.$$

The corresponding energies are $E_P=(2/m_0)P^2$ and $E_{PX}=(2/m_0)P_X^2$. The coefficients $\mathfrak{A}$, $\mathfrak{B}$, $\mathfrak{C}$, $\mathfrak{A}_\Delta$, $\mathfrak{B}_\Delta$, and $\mathfrak{C}_\Delta$ for VB and the same ones for CB ($\mathfrak{A}_C$, $\mathfrak{B}_C$, $\mathfrak{C}_C$, $\mathfrak{A}_{\Delta C}$, $\mathfrak{B}_{\Delta C}$, $\mathfrak{C}_{\Delta C}$) are given by

$$\mathfrak{A}=\tilde{\gamma}_2(2\check{k}_z^2-\check{k}_\rho^2);\quad \mathfrak{A}_\Delta=\tilde{\gamma}_{\Delta 2}(2\check{k}_z^2-\check{k}_\rho^2),$$

$$\mathfrak{B}=2\sqrt{3}\tilde{\gamma}_3\check{k}_z\check{k}_-;\quad \mathfrak{B}_\Delta=2\sqrt{3}\tilde{\gamma}_{\Delta 3}\check{k}_z\check{k}_-,$$

$$\mathfrak{C}=\sqrt{3}[\tilde{\gamma}_2(\check{k}_x^2-\check{k}_y^2)-2i\tilde{\gamma}_3\check{k}_x\check{k}_y];\quad \mathfrak{C}_\Delta=\sqrt{3}[\tilde{\gamma}_{\Delta 2}(\check{k}_x^2-\check{k}_y^2)-2i\tilde{\gamma}_{\Delta 3}\check{k}_x\check{k}_y],$$

$$\mathfrak{A}_C=\tilde{\gamma}_{C2}(2\check{k}_z^2-\check{k}_\rho^2);\quad \mathfrak{A}_{\Delta C}=\tilde{\gamma}_{\Delta C2}(2\check{k}_z^2-\check{k}_\rho^2),$$

$$\mathfrak{B}_C=2\sqrt{3}\tilde{\gamma}_{C3}\check{k}_z\check{k}_-;\quad \mathfrak{B}_{\Delta C}=2\sqrt{3}\tilde{\gamma}_{\Delta C3}\check{k}_z\check{k}_-,$$

$$\mathfrak{C}_C=\sqrt{3}[\tilde{\gamma}_{C2}(\check{k}_x^2-\check{k}_y^2)-2i\tilde{\gamma}_{C3}\check{k}_x\check{k}_y];\quad \mathfrak{C}_{\Delta C}=\sqrt{3}[\tilde{\gamma}_{\Delta C2}(\check{k}_x^2-\check{k}_y^2)-2i\tilde{\gamma}_{\Delta C3}\check{k}_x\check{k}_y].$$

The parameters $\tilde{\gamma}_1$, $\tilde{\gamma}_2$, $\tilde{\gamma}_3$, $\tilde{\gamma}_{\Delta 1}$, $\tilde{\gamma}_{\Delta 2}$, and $\tilde{\gamma}_{\Delta 3}$ are the modified Luttinger parameters[37] which are related to the Luttinger parameters[38] $(\gamma_1,\gamma_2,\gamma_3)$ by

$$\tilde{\gamma}_1=\gamma_1-\frac{1}{3}\frac{E_P}{E_G}-\frac{E_{PX}}{3}\left\{\frac{1}{E_G+E_{GC}+\Delta_C}+\frac{1}{E_G+E_{GC}}\right\},$$

$$\tilde{\gamma}_2=\gamma_2-\frac{1}{6}\frac{E_P}{E_G}+\frac{1}{6}\frac{E_{PX}}{E_G+E_{GC}},$$

$$\tilde{\gamma}_3=\gamma_3-\frac{1}{6}\frac{E_P}{E_G}-\frac{1}{6}\frac{E_{PX}}{E_G+E_{GC}},$$

$$\tilde{\gamma}_{\Delta 1}=\gamma_1-\frac{1}{3}\frac{E_P}{E_G}-\frac{E_{PX}}{3}\left\{\frac{1}{E_G+E_{GC}}+\frac{1}{E_G+E_{GC}+\Delta_C}-\frac{2}{\Delta+E_G+E_{GC}+\Delta_C}\right\},$$

$$\tilde{\gamma}_{\Delta 2}=\gamma_2-\frac{E_P}{6E_G}+\frac{E_{PX}}{12}\left\{\frac{2}{E_G+E_{GC}}-\frac{1}{E_G+E_{GC}+\Delta_C}-\frac{1}{\Delta+E_G+E_{GC}+\Delta_C}\right\},$$

$$\tilde{\gamma}_{\Delta 3}=\gamma_3-\frac{E_P}{6E_G}-\frac{E_{PX}}{12}\left\{\frac{2}{E_G+E_{GC}}-\frac{1}{E_G+E_{GC}+\Delta_C}-\frac{1}{\Delta+E_G+E_{GC}+\Delta_C}\right\}.$$

In the same way, for *p*-type CB's we define the modified Luttinger parameters $\tilde{\gamma}_{C1},\tilde{\gamma}_{C2},\tilde{\gamma}_{C3},\tilde{\gamma}_{\Delta C1},\tilde{\gamma}_{\Delta C2},\tilde{\gamma}_{\Delta C3}$ and for *s*-type CB we also define the $\tilde{\gamma}_C$ ones as follows:

$$\tilde{\gamma}_{C1}=\gamma_{C1}+\frac{E_{PX}}{3}\left\{\frac{1}{\Delta_C+E_G+E_{GC}}+\frac{1}{\Delta_C+E_G+E_{GC}+\Delta}\right\},$$

$$\tilde{\gamma}_{C2}=\gamma_{C2}-\frac{1}{6}\frac{E_{PX}}{\Delta_C+E_{GC}+E_G+\Delta},$$

$$\tilde{\gamma}_{C3}=\gamma_{C3}+\frac{1}{6}\frac{E_{PX}}{\Delta_C+E_{GC}+E_G+\Delta},$$

$$\tilde{\gamma}_{\Delta C1}=\gamma_{C1}+\frac{E_{PX}}{3}\left\{\frac{1}{\Delta_C+E_G+E_{GC}}+\frac{1}{\Delta_C+E_G+E_{GC}+\Delta}-\frac{2}{E_G+E_{GC}}\right\},$$

$$\tilde{\gamma}_{\Delta C2}=\gamma_{C2}+\frac{E_{PX}}{12}\left\{\frac{1}{\Delta_C+E_G+E_{GC}}+\frac{1}{E_G+E_{GC}}-\frac{2}{\Delta_C+E_G+E_{GC}+\Delta}\right\},$$

$$\tilde{\gamma}_{\Delta C3}=\gamma_{C3}-\frac{E_{PX}}{12}\left\{\frac{1}{\Delta_C+E_G+E_{GC}}+\frac{1}{E_G+E_{GC}}-\frac{2}{\Delta_C+E_G+E_{GC}+\Delta}\right\},$$

$$\tilde{\gamma}_C=\gamma_C-\frac{E_P}{3}\left\{\frac{2}{E_G}+\frac{1}{E_G+\Delta}\right\},$$

where $(\gamma_{C1},\gamma_{C2},\gamma_{C3})$ and γ_C are the Luttinger-like parameters associated to the *p*-type CB and *s*-type CB, respectively.

APPENDIX B: BASIS FUNCTIONS

This appendix gives the basis used in our calculations. In order to contract the writing script, we use the following notations:

Inside Γ_8^- CB, we note the functions $|\frac{3}{2},M\rangle_{\Gamma_8^-}$ like $|cM\rangle$, where $M=\pm\frac{3}{2},\pm\frac{1}{2}$.

Inside Γ_6^- CB, we note the functions $|\frac{1}{2},\pm\frac{1}{2}\rangle_{\Gamma_6^-}$ like $|c\pm\frac{7}{2}\rangle$.

Inside Γ_7^- CB, we note the functions $|S\uparrow\rangle$ and $|S\downarrow\rangle$ like $|+\rangle$ and $|-\rangle$, respectively.

Inside Γ_8^+ VB, we note the functions $|\frac{3}{2},M\rangle_{\Gamma_8^+}$ like $|M\rangle$ where $M=\pm\frac{3}{2},\pm\frac{1}{2}$.

Inside Γ_7^+ CB, we note the functions $|\frac{1}{2},\pm\frac{1}{2}\rangle_{\Gamma_7^+}$ like $|\pm\frac{7}{2}\rangle$.

In semiconductors, we replace the atomic functions *s*, *x*, *y*, *z*,x_c,y_c,z_c by the functions *S*, *X*, *Y*, *Z*,X_C,Y_C, Z_C which are defined as

$$H_{\mathfrak{U}}X_C = E_{X_C}X_C; \quad H_{\mathfrak{U}}Y_C = E_{X_C}Y_C; \quad H_{\mathfrak{U}}Z_C = E_{X_C}Z_C,$$

$$H_{\mathfrak{U}}S = E_S S,$$

$$H_{\mathfrak{U}}X = E_X X; \quad H_{\mathfrak{U}}Y = E_X Y; \quad H_{\mathfrak{U}}Z = E_X Z,$$

where $H_{\mathfrak{U}}$ is given by $P^2/2m_0 + \mathfrak{U}$ and E_{X_C}, E_S, E_X are the eigenenergies for *p*-type CB, *s*-type CB, and *p*-type VB, respectively. These eigenenergies for the CB and VB are considered well known. Periodic functions S and X,Y,Z,X_C,Y_C,Z_C are assumed to be real and to transform like *s*-like and *p*-like atomic functions under operations of the cubic symmetry group (O_H). The X_C, Y_C, Z_C functions denote the conduction *p*-type levels whereas, the X,Y,Z functions denote the valence *p*-type levels. The basis functions are defined by analogy with the atomic ones (Table III).

[1] B.F. Levine, K.K. Choi, C.G. Bethea, J. Walker, and R.J. Malik, Appl. Phys. Lett. **50**, 1092 (1987).

[2] B.F. Levine, C.G. Bethea, G. Hasnain, J. Walker, and R.J. Malik, Appl. Phys. Lett. **53**, 296 (1988).

[3] B.F. Levine, C.G. Bethea, G. Hasnain, V.O. Shen, E. Pelve, and P.R. Abboh, Appl. Phys. Lett. **56**, 851 (1990).

[4] S.D. Gunapala, B.F. Levine, D. Ritter, R. Hamm, and M.B. Panish, Appl. Phys. Lett. **58**, 2024 (1991).

[5] B.F. Levine, S.D. Gunapala, G.M. Kuo, S.S. Pei, and S. Hui, Appl. Phys. Lett. **59**, 1864 (1991).

[6] L.C. West and S.J. Eglash, Appl. Phys. Lett. **46**, 1156 (1985).

[7] Y.C. Chang and R.B. James, Phys. Rev. B **39**, 12 672 (1989).

[8] J.S. Park, P.G. Karunasiri, and K.L. Wang, Appl. Phys. Lett. **60**, 103 (1992).

[9] J.M. Berroir, S. Zanier, Y. Guldner, J.P. Vieren, I. Sagnes, F. Glowachi, Y. Campidelli, and P.A. Badoz, in *Semiconductor Heteroepitaxy: Growth, Characterization and Device Applications*, edited by B. Gil (World Scientific, Singapore, 1995), p. 314.

[10] R.G. Karunasiri, J.S. Park, and K.L. Wang, Appl. Phys. Lett. **61**, 2434 (1992).

[11] R. People, J.C. Bean, S.K. Sputz, C.G. Bethea, and L.J. Peticolas, Thin Solid Films **222**, 120 (1992).

[12] S.K. Chun, D.S. Pan, and K.L. Wang, Phys. Rev. B **47**, 15 638 (1993).

[13] P. Boucaud, L. Gao, Z. Moussa, F. Visocekas, F.H. Julien, J.M. Lourtioz, I. Sagnes, Y. Campidelli, and P.A. Badoz, Appl. Phys. Lett. **67**, 2948 (1995).

[14] L. Wu, P. Boucaud, J.M. Lourtioz, F.H. Julien, I. Sagnes, Y. Campidelli, and P.A. Badoz, Appl. Phys. Lett. **67**, 3462 (1995).

[15] M. Seto, M. Helm, Z. Moussa, P. Boucaud, F.H. Julien, J.M. Lourtioz, J.F. Nützel, and G. Abstreiter, Appl. Phys. Lett. **65**, 2969 (1994).

[16] P. Boucaud, F.H. Julien, R. Prazeres, J.M. Ortega, I. Sagnes, and Y. Campidelli, Appl. Phys. Lett. **69**, 3069 (1996).

[17] P. Boucaud, L. Wu, C. Guedj, F.H. Julien, I. Sagnes, Y. Campidelli, and L. Garchery, J. Appl. Phys. **80**, 1414 (1996). See also E. Dekel, E. Ehrenfreud, D. Gershoni, P. Boucaud, I. Sagnes, and Y. Campidelli, Phys. Rev. B **56**, 15 734 (1997).

[18] E. Corbin, K.B. Wong, and M. Jaros, Phys. Rev. B **50**, 2339 (1994).

[19] I. Fromherz, E. Koppensteiner, M. Helm, G. Bauer, J.F. Nützel, and G. Abstreiter, Phys. Rev. B **50**, 15 073 (1994).

[20] S. Zanier, J.M. Berroir, Y. Guldner, J.P. Vieren, I. Sagnes, F. Glowachi, Y. Campidelli, and P.A. Badoz, Phys. Rev. B **51**, 14 311 (1995).

[21] P. Pfeffer and W. Zawadski, Phys. Rev. B **41**, 1561 (1990).

[22] G. Fishman, Phys. Rev. B **52**, 11 132 (1995).

[23] D. Brinkman, A. Löffler, and G. Fishman, *Fourth International Conference on Optics of Excitons in Confined Systems* [Nuovo Cimento **17**, 1389 (1995)].

[24] D. Brinkman, G. Fishman, C. Gourgon, Le Si Dang, A. Löffler, and H. Mariette, Phys. Rev. B **53**, 1872 (1996).

[25] E.O. Kane, in *Handbook on Semiconductors*, edited by T. S. Moss (North-Holland, Amsterdam, 1982), p. 193.

[26] A. Mycielski, J. Kossut, M. Dobrowolska, and W. Dobrowolski, J. Phys. C **15**, 3293 (1982), p. 193.

[27] U. Rössler, Solid State Commun. **49**, 943 (1984).

[28] M. Cardona, N.E. Christensen, and G. Fasol, Phys. Rev. B **38**, 1806 (1988).

[29] G.E. Pikus, Izv. Akad. Nauk SSSR, Ser. Fiz. **52**, 493 (1988).

[30] P. Pfeffer, and W. Zawadski, Phys. Rev. B **53**, 12 813 (1996).

[31] E.O. Kane, J. Phys. Chem. Solids **1**, 249 (1957). See also E.O. Kane, in *Semiconductors and Semimetals*, edited by R.K. Willardson and A.C. Beer (Academic, New York, 1966), Vol. 1.

[32] G.E. Pikus and G.L. Bir, Fiz. Tverd. Tela (Leningrad) **1**, 1642 (1959) [Sov. Phys. Solid State **1**, 1502 (1960)]. See also G.L. Bir and G.E. Pikus, *Symmetry and Strain-Induced Effects in Semiconductors* (Wiley, New York, 1974).

[33] See, for example, Thomas B. Bahder, Phys. Rev. B **41**, 11 992 (1990).

[34] *Semiconductors, Physics Group IV Elements and III-V Compounds*, edited by O. Madelung, M. Schultz, and H. Weiss, Landolt-Börnstein, New Series Group III, Vol. 17, Pt.a (Springer-Verlag, New York, 1982).

[35] R. People, IEEE J. Quantum Electron. **QE22**, 1696 (1986).

[36] A. Twardowski and C. Hermann, Phys. Rev. B **35**, 8144 (1987). See also M. Altarelli, U. Ekenberg, and A. Fasolino, *ibid.* **32**, 5138 (1985).

[37] K. Boujdaria, S. Ridene, and G. Fishman, Phys. Rev. B **63**, 235 302 (2001).

[38] J.M. Luttinger, Phys. Rev. **102**, 1030 (1956).

[39] K. Boujdaria (unpublished).